Modelling the pressure field in the vicinity of a microphone membrane using PIV

O. Richoux [a,*], A. Degroot [a], B. Gazengel [a], R. MacDonald [b], M. Campbell [b]

[a] LAUM, CNRS, Université du Maine, Av. O. Messiaen, 72085 Le Mans, France
[b] Acoustics and Fluid dynamics Group, School of Physics, University of Edinburgh Kings Buildings, Edinburgh, UK

ARTICLE INFO

ABSTRACT

A new approach for estimating the acoustic pressure in the near field of a microphone based on non-intrusive direct measurement of acoustic particle velocity is proposed.

This method enables the estimation of the acoustic pressure inside a domain located in front of the microphone membrane. The acoustic pressure is calculated using the acoustic particle velocity on the frontiers of this domain and a physical model based on the Green function of the system.

Results are obtained using the acoustic velocity measured with Particle Image Velocimetry (PIV) in front of a microphone excited with a plane wave inside a rectangular waveguide. They show that the diffraction of the plane wave by the microphone leads to an increase of the acoustic pressure on the microphone edge in the order of magnitude of 0.1 dB.

1. Introduction

Over the years, several methods have been developed for microphone calibration (for a review see [1]). These methods can be classified into two sorts: (i) relative calibration which provides an estimate of the sensitivity of a microphone as a function of a reference sensitivity and (ii) absolute calibration [2] which leads to an estimation of the sensitivity without any reference microphone.

For absolute calibration, the reciprocity technique is usually used which provides a typical precision of around 0.05 dB in an enclosed field configuration. In a free field configuration, this technique has been adapted [3,4] and standardized [5]. Nevertheless, free field absolute calibration suffers from numerous problems which are not resolved at present: the location of the acoustic center of the microphone is crucially important [6], the generation of standing waves between the different microphones perturbs the measurements and, generally, external reflections disturb the acoustic field in the vicinity of the microphone.

Microphone calibration using non-intrusive optical techniques such as laser Doppler Velocimetry is proposed by some authors. These studies are mainly conducted in enclosed field conditions, more precisely in waveguides excited with plane waves. Two approaches are used.

On the one hand, authors consider that the impedance of the medium is known and measure the acoustic velocity at a single point. This supposes that the boundary conditions of the medium are perfectly known. We call it the "global approach". In this case, the acoustic pressure can be estimated at the measurement point thanks to the impedance. Acoustic pressure can also be estimated elsewhere using a propagation model of the system under study. Taylor [7], MacGillivray [8,9] and Koukoulas et al. [10] use this approach. First results are encouraging: Taylor [7] shows that this method is accurate within ± 0.03 dB at 500 Hz, MacGillivray et al. [8,9] reach an accuracy of around 0.1 dB and Koukoulas et al. [10] propose an accuracy of 0.2 dB at 170 Hz.

On the other hand, authors consider a volume of fluid and measure the acoustic velocity on the volume boundaries. A propagating model of the fluid enables the estimation of the acoustic pressure everywhere in the volume. We call this the "local approach". For plane waves a slice of fluid is considered and the acoustic velocity measured at two points to estimate the acoustic pressure in the middle of the slice. Degroot et al. [11] use this approach and show that using a $(u–u)$ probe with two LDV measurements provides a minimum uncertainty on the pressure estimation of 0.013 dB for frequencies of 1360 Hz and 680 Hz.

The approaches described above for enclosed field calibration could be used in a free field. The first (global) approach only requires the measurement of the acoustic velocity at a single point but also requires that the impedance of the fluid for free field

conditions is known. This can only be the case if the boundary conditions of the system are perfectly known, for example in a semi-infinite domain which can be reproduced with a semi anechoïc chamber. The second (local) approach does not require the boundary conditions of the system under study to be known but instead the acoustic velocity must be measured at a number of locations near the microphone membrane, in order to estimate the acoustic pressure on the membrane.

The local approach requires the characterization of the acoustic nearfield of a structure by LDV or other non-intrusive techniques. Previous work has been done by Gazengel et al. [12], who measure the acoustic particle velocity in front of a loudspeaker to characterize its acoustic radiation in a free field using the LDV technique. Schedin et al. [13] propose measuring the acoustic particle velocity in the vicinity of a plate using two-reference-beam double-pulsed holographic interferometry and Moreau et al. characterize the acoustic field in a waveguide boundary layer using LDV and PIV techniques [14].

In this paper, we propose a preliminary study for calibrating microphones in free field conditions using a non-intrusive measurement technique and the local approach described above. Section 2 presents the general method used for estimating the acoustic pressure on the microphone membrane using the acoustic velocity measured at many locations near the membrane. Section 3 presents the experimental study of the acoustic field in the close vicinity of a microphone. In this section, the acoustic particle velocity is measured using a PIV technique. In the fourth section, a 2D model of the acoustic field near the microphone in derived using the Green function of the volume under study. Finally, the acoustic pressure field is estimated in front of the microphone membrane using the measured acoustic velocity and some discussion is given.

2. General formulation of the acoustic pressure field in the vicinity of a microphone membrane

In this section, a microphone excited with a plane wave is studied. An analytical development of the pressure field is proposed, considering a fluid domain (air) located in front of the microphone membrane (see Fig. 1). Acoustic pressure inside this volume can be estimated at the position $(r, \theta, z) = (\vec{w}, z)$ by means of measurement of normal velocity on the volume boundaries with an integral formulation.
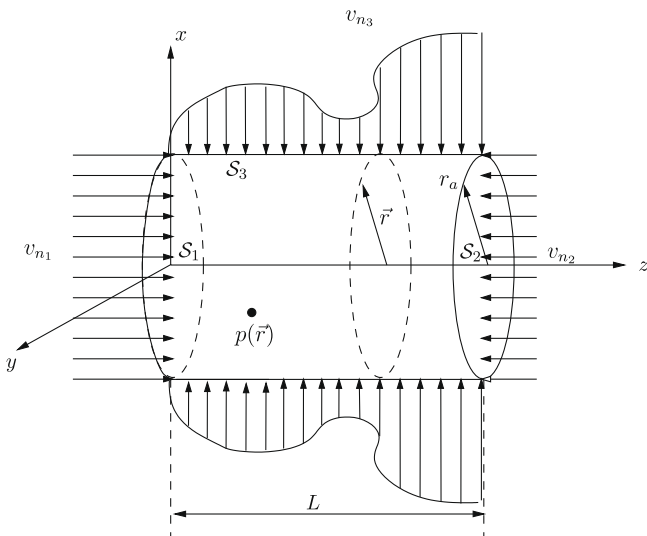

Fig. 1. Studied volume in front of the microphone.

The system under study (see Fig. 1) is an air fluid column with length L and a circular section of radius r_a. The circular sections (S_1, S_2) and the surface of the fluid column S_3 are subjected respectively to the normal acoustic velocities v_{n_1}, v_{n_2} and v_{n_3}. As described in Fig. 1 and according to experimental results presented in Section 3, the normal acoustic velocities v_{n_1} and v_{n_2} are chosen to be uniform on the circular section and v_{n_3} is considered to vary on the section S_3.

A general integral formulation of the acoustic pressure in the volume V is proposed hereafter.

In the frequency domain the acoustic pressure $p(\vec{r}, t)$ is written as

$$p(\vec{r}, t) = p(\vec{r})e^{j\omega t}, \tag{1}$$

where ω is the acoustic pulsation defined by $\omega = 2\pi f$. In the linear acoustic approximation and in the case of a perfect fluid, the acoustic propagation in the air fluid column V, is given by

$$(\Delta + k^2)p(\vec{r}) = 0, \tag{2}$$

where $k = \omega/c_0$ is the wave number and c_0 is the sound celerity. The boundary conditions associated with Eq. (2) are written

$$\frac{\partial p(\vec{r})}{\partial n} = -j\omega\rho v_{n_1}(r) \quad \text{for } r \in (0, r_a), \ \theta \in (0, 2\pi), \ z = 0, \tag{3}$$

$$\frac{\partial p(\vec{r})}{\partial n} = -j\omega\rho v_{n_2}(r) \quad \text{for } r \in (0, r_a), \ \theta \in (0, 2\pi), \ z = L, \tag{4}$$

$$\frac{\partial p(\vec{r})}{\partial n} = -j\omega\rho v_{n_3}(r) \quad \text{for } r = r_a, \ \theta \in (0, 2\pi), \ z \in (0, L), \tag{5}$$

where ρ is the air density and $\partial/\partial n = \partial_n$ is the normal derivative to the surface S. The acoustic pressure field $p(\vec{r})$ in the volume V (described by the closed surface S) is written, in this integral form,

$$p(\vec{r}) = \int\int\int_V G(\vec{r}, \vec{r}_0)f(\vec{r}_0)dV_0 + \int\int_S [G(\vec{r}, \vec{r}_0)\partial n_0 p(\vec{r}_0)$$
$$- p(\vec{r}_0)\partial n_0 G(\vec{r}, \vec{r}_0)]dS_0, \tag{6}$$

where the function $f(\vec{r}_0)$ describes the sources distributed inside the volume V and $G(\vec{r}, \vec{r}_0)$ is the Green function defined by the following equation:

$$(\Delta + k^2)G(\vec{r}, \vec{r}_0) = -\delta(\vec{r} - \vec{r}_0) \text{ in } V, \tag{7}$$

and the boundary conditions on the surface S. In Eq. (7), $\delta(\vec{r} - \vec{r}_0)$ is the Dirac distribution. The boundary conditions for the Green function are chosen as

$$\partial_{n_0} G(\vec{r}, \vec{r}_0) = 0 \quad \text{for } r \in (0, r_a), \ \theta \in (0, 2\pi), \ z = 0, \tag{8}$$

$$\partial_{n_0} G(\vec{r}, \vec{r}_0) = 0 \quad \text{for } r \in (0, r_a), \ \theta \in (0, 2\pi), \ z = L, \tag{9}$$

$$\partial_{n_0} G(\vec{r}, \vec{r}_0) = 0 \quad \text{for } r = r_a, \ \theta \in (0, 2\pi), \ z \in (0, L), \tag{10}$$

to allow a description of the acoustic pressure field as a function of the acoustic velocity on the boundaries. Using Eqs. (7)–(10), Eq. (6), without any sources ($f(\vec{r}_0) = 0$), is written

$$p(\vec{r}) = \int\int_S G(\vec{r}, \vec{r}_0)\partial n_0 p(\vec{r}_0)dS_0. \tag{11}$$

Eq. (11) combined with Eqs. (3)–(5) leads to the following expression for the acoustic pressure in the volume V

$$p(\vec{r}) = -j\omega\rho \int\int_S G(\vec{r}, \vec{r}_0) v_{n_0} dS_0$$
$$= -j\omega\rho \sum_i \int\int_{S_i} G(\vec{r}, \vec{r}_0) v_{n_i} dS_i, \tag{12}$$

where $i = 1, 2,$ and 3. Knowing the acoustic velocity on the surface $S_1, S_2,$ and S_3 and the Green function of the system, the acoustic pressure can determined in the volume V with the Eq. (12).

3. Experimental characterization of the acoustic velocity field in the vicinity of a microphone membrane

In this section, the acoustic velocity field is estimated experimentally using Particle Image Velocimetry (PIV) inside the domain close to the microphone membrane as shown in Fig. 1. The microphone is positioned inside a waveguide. PIV has previously been used to study acoustic flow in a waveguide [14]. The acoustic velocity field is measured inside a plane region (laser sheet) of dimensions $2r_{a*} L$.

3.1. Experimental set-up

3.1.1. PIV system

The PIV system uses a pulsed Cu-Laser Oxford Lasers LS20-50 with a time between pulses of 20 µs. The mean power of the laser is 20 W and each pulse has a duration of 25–30 ns with a wavelength of 510.6 nm (green). The beam from the laser is converted to a light sheet for delivery to the region of interest. A CCD camera (Sensicam Double Shutter) is used for the acquisition of the PIV images, with a resolution 1280 × 1024 pixels. A Berkley Nucleonics model 500 A pulse generator is used in conjunction with National Instruments LabVIEW software to allow the capture of PIV image pairs at any phase in the period of the acoustic cycle. Thirty measurements are made at a given phase and averaged to estimate the velocity field. Cross-correlation and post-processing are carried out on in-house PIV software.

3.1.2. Acoustic system

The experimental set-up is made up of a JBL 2446H loudspeaker mounted on a closed Perspex tube (with 10 mm wall thickness) with a length $L = 0.5$ m and a square section $S = 0.1 \times 0.1$ m^2. The first cut-off frequency is 1720 Hz (first transverse mode). In the waveguide, a 1 in. B&K microphone is placed parallel to the guide axis. Fig. 2 shows the acoustic set-up and the PIV system.

A stationary plane wave with a frequency $f = 680$ Hz is established in the waveguide. The microphone membrane is located between a node and an antinode of acoustic velocity to measure a sufficient acoustic velocity amplitude for PIV. The light sheet position is adjusted so as to graze the microphone membrane, in a plane corresponding to the diameter of the membrane. The waveguide is "seeded" using a SAFEX fog machine. The seeding is introduced during 3–5 s and 10–15 min are required before doing the measurement. The CCD Camera is positioned perpendicular to the light sheet and focused on the illuminated fog particles. The
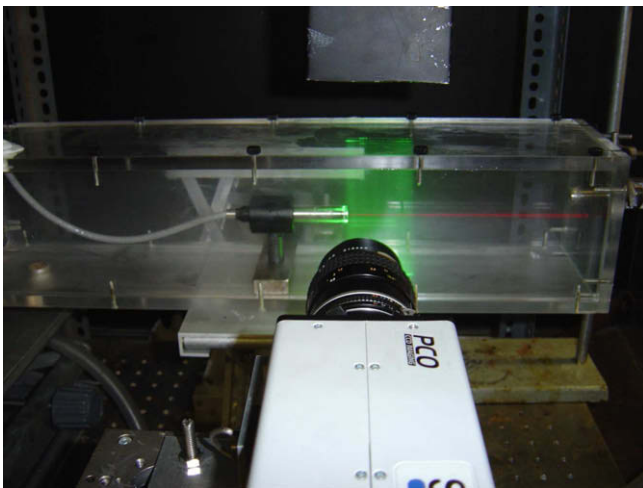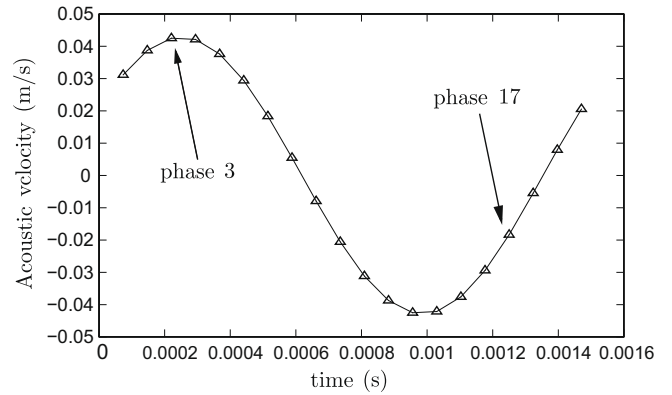

Fig. 3. View of the 20 measurement phases during one acoustic period.

observation window corresponds to a rectangular section of the volume under study (dimensions $2r_a \times L$). Measurements are realized for 20 equally spaced phase steps in the acoustic period (see Fig. 3).

3.2. Experimental results

3.2.1. General analysis

The acoustic velocity field measured for the phase 3 of the acoustic period is shown on the Fig. 4. The z-axis is the guide axis. The dimensions of the PIV image are 0.02×0.024 m^2. This PIV image highlights the evolution of the acoustic velocity field streamlines at the vicinity of the microphone membrane. In this representation, the velocity vectors go toward the membrane for a positive velocity amplitude. The shape of the field lines are approximately symmetrical around the microphone axis.

3.2.2. Longitudinal acoustic velocity

Fig. 5 shows the longitudinal acoustic velocity v_z as a function of r for $z = 0$ m and for $z = 0.015$ m. In this figure, the microphone membrane is located at $z = 0.015$ m. This figure shows that the longitudinal velocity amplitude is almost constant for $z = 0$. The acoustic wave can therefore be considered to be plane at this position (corresponding to surface S_1, see Fig. 1) in the domain under study. However, velocity v_{n1} shows a variation of $\pm 5.10^{-3}$ m s^{-1} around the mean value (5.10^{-2} m s^{-1}), which introduces an uncertainty in the pressure estimation.

In the very closed vicinity of the microphone (the region defined by $r \in [-0.004; 0.004]$ m and $z \in [0.013; 0.015]$ m), the acoustic
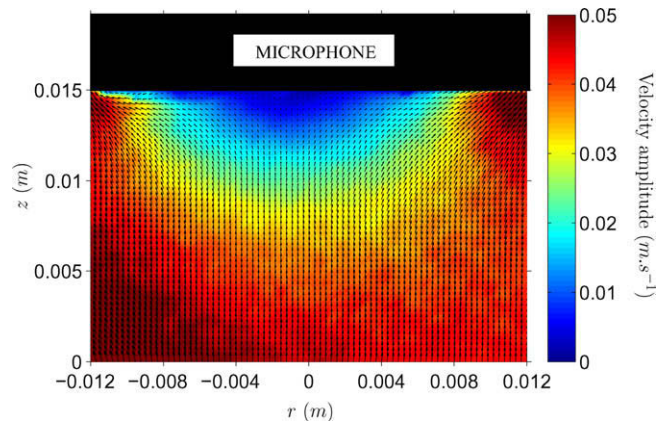

Fig. 2. Experimental set-up.

Fig. 4. View of experimental acoustic velocity field in the vicinity of the microphone for phase 3.

Fig. 5. Acoustic velocity amplitude v_z as a function of r for $z = 0$ m (a) and $z = 0.015$ m (b).
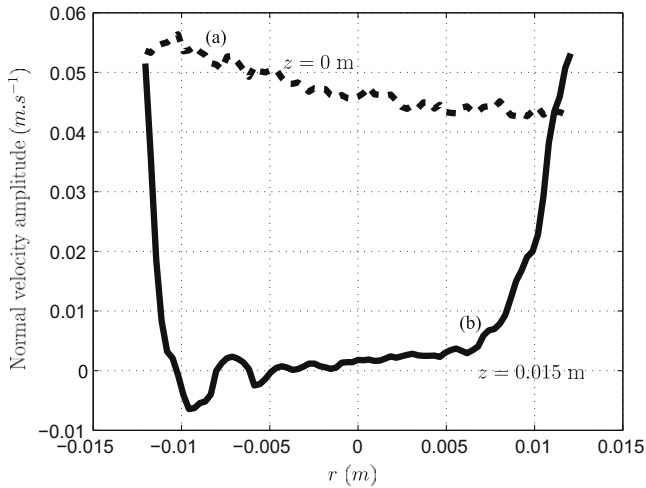

Fig. 7. Acoustic velocity amplitude v_r as a function of z for $r = 0$ m (a) and $r = 0.012$ (b).

velocity field vanishes due to the membrane stiffness. For $r = 0$, the amplitude of the acoustic velocity v_z decreases from 0.045 m s^{-1}($z = 0$ m) to 2.10^{-3} m s^{-1}($z = 0.015$ m). Assuming the membrane velocity equals the acoustic velocity at $z = 0.015$ m, this result shows that the membrane velocity is very small compared with the acoustic velocity (ratio $\simeq 1/22$) measured at $z = 0$ (15 mm from the membrane). This result should be confirmed by complementary direct measurements of the membrane velocity. In further works, the microphone membrane velocity should be measured by means of a Laser Vibrometer in order to confirm this hypothesis.

3.2.3. Radial acoustic velocity

Fig. 6A shows the radial acoustic velocity amplitude v_r as a function of r for $z = 0$ m and $z = 0.015$ m. In the very close vicinity of the membrane, the acoustic velocity amplitude v_r increases with r. At $z = 0.015$ m and for $r = 0$ m, the radial acoustic velocity amplitude is $v_r = 1.10^{-4}$ m s^{-1} and for $r = 0.011$ m, $v_r = 0.45$ m s^{-1}. v_r is maximum for $r = 0.012$ m which illustrates the acoustic leakage at the edge of the microphone. In the vicinity of the microphone, the distribution of the radial velocity amplitude is not exactly symmetric (Fig. 6A). This asymmetry can be due to microphone misalignment, error in the velocity estimation with PIV or a weak air
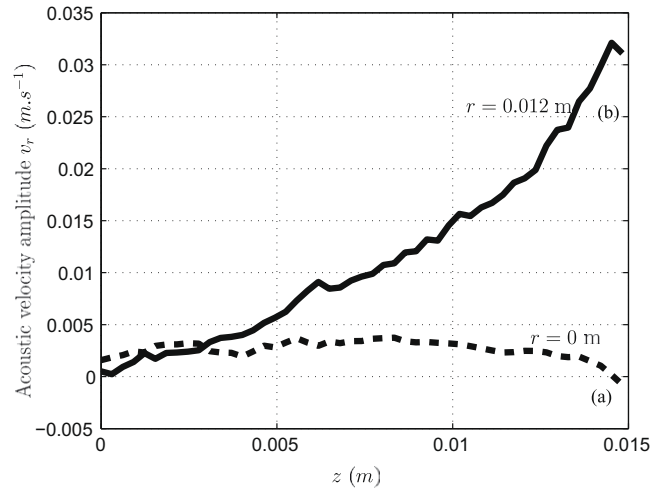
current caused by thermal effects. For greater distance from the microphone ($z < 0.015$ m), the radial velocity amplitude becomes symmetric as shown on Fig. 6B.

Finally, Fig. 7 illustrates the radial acoustic velocity amplitude v_r as a function of z for $r = 0$ m and $r = 0.012$ m corresponding to surface S_3 shown in Fig. 1. The radial acoustic velocity amplitude increases from zero ($r = 0$ m) to 0.033 m s^{-1} ($r = 0.012$ m).

This phenomenon illustrates again the presence of acoustic leakage on the edge of the microphone and has to be taken into account in Eq. (12).

Taking these experimental results into account, we consider in the following that the longitudinal velocity v_{n_1} is constant, that the membrane velocity v_{n_2} can be neglected ($v_{n_2} = 0$) and that the radial velocity v_{n_3} depends on the z coordinate. The profile of v_{n_3} as a function of z is estimated analytically in the following (Section 5).

4. Analytical model of the acoustic pressure field in the vicinity of a microphone membrane

In this section, we derive a specific expression of acoustic pressure in volume V using the normal velocity profiles v_{n_1} and v_{n_3} estimated from experimental results (Section 3). We assume an
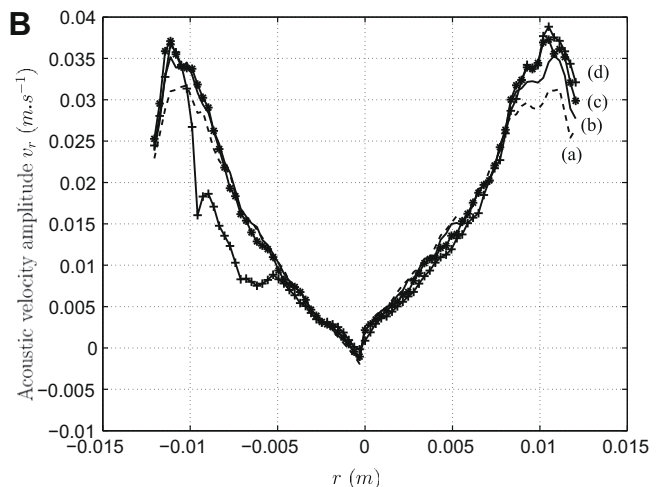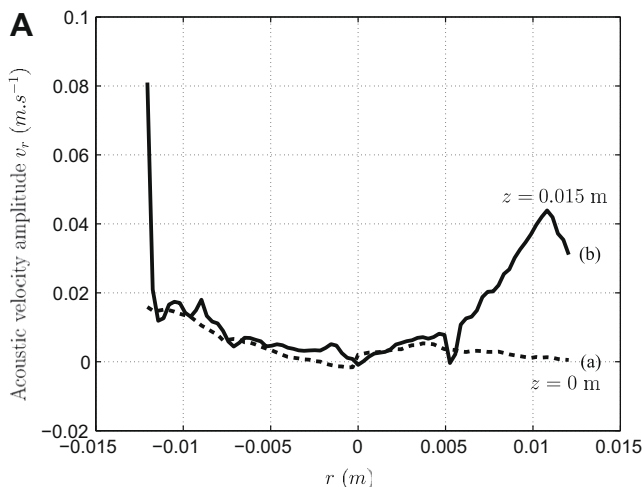

Fig. 6. (A) Radial acoustic velocity amplitude v_r as a function of r for $z = 0$ m (a) and $z = 0.015$ (b). (B) Radial acoustic velocity amplitude v_r as a function of r for (a) $z = 0.0136$ m (...), (b) $z = 0.0139$ m (– –), (c) $z = 0.0142$ m (*), and (d) $z = 0.0145$ (+).

axial symmetry of the system, which allows the derivation of a 2D model of the acoustic field.

4.1. Green function of the system

The Green function $G(\vec{r}, \vec{r}_0)$ solution of the problem described by Eq. (7), can be presented as

$$(\Delta_{\vec{w}} + \delta_z + k^2)G(\vec{w}, z; \vec{w}_0, z_0) = -\delta(\vec{w} - \vec{w}_0)\delta(z - z_0) \text{ in } V, \quad (13)$$

where $\Delta_{\vec{w}} = (1/r)\partial_r(r\partial_r) + (1/r2)\partial_\theta 2$. The boundary conditions (Eqs. (8)–(10)) are expressed as following:

$$\partial_{n_0}G(\vec{r}, \vec{r}_0) = \partial_{z_0}G(\vec{w}, z; \vec{w}_0, z_0) = 0 \quad \text{for } z = 0, \quad (14)$$

$$\partial_{n_0}G(\vec{r}, \vec{r}_0) = \partial_{z_0}G(\vec{w}, z; \vec{w}_0, z_0) = 0 \quad \text{for } z = L, \quad (15)$$

$$\partial_{n_0}G(\vec{r}, \vec{r}_0) = \partial_{r_0}G(\vec{w}, z; \vec{w}_0, z_0) = 0 \quad \text{for } r = r_a. \quad (16)$$

The Green function $G(\vec{w}, z; \vec{w}_0, z_0)$ can be written as a discrete sum of eigenfunctions $\Psi_{\mu\nu}(\vec{w})$ of the cylinder V under the form

$$G(\vec{w}, z; \vec{w}_0, z_0) = \sum_{\mu,\nu=0}^{\infty} g_{\mu\nu}(z, z_0)\Psi_{\mu\nu}(\vec{w}_0\Psi_{\mu\nu}(\vec{w}), \quad (17)$$

where $g_{\mu,\nu}(z, z_0)$ are dependent on the position z and $\Psi_{\mu\nu}(\vec{w})$ are solutions of the following problem:

$$(\Delta_{\vec{w}} + k_{w\mu\nu}^2)\Psi_{\mu\nu}(\vec{w}) = -\delta(\vec{w} - \vec{w}_0)\forall r \in (0, r_a)$$
$$\text{and} \quad \forall\theta \in (0, 2\pi), \quad (18)$$

$$\partial_n\Psi_{\mu\nu}(\vec{w}) = 0 \text{ for } r = r_a \text{ and } \forall\theta \in (0, 2\pi). \quad (19)$$

The eigenfunctions $\Psi_{\mu\nu}(\vec{w}) = \Psi_{\mu\nu}(r, \theta)$ take the following form

$$\Psi_{\mu\nu}(r, \theta) = A_{\mu\nu}\cos(\mu\theta)J_\mu(k_{w\mu\nu}r), \quad (20)$$

where J_μ is the Bessel function and the eigenvalues $k_{w\mu\nu}$ are given by

$$k_{w\mu\nu} = \frac{\gamma_{\mu\nu}}{r_a}, \quad \text{with } J'_\mu(\gamma_{\mu\nu}) = 0. \quad (21)$$

The coefficients $A_{\mu\nu}$ are found using the orthogonality of the eigenfunctions and are expressed as

$$A_{\mu\nu} = \frac{2}{(1 + \delta_{\mu0})\pi r_a 2\left(1 - \frac{\mu2}{\gamma_{\mu\nu}2}\right)J2_\mu(\gamma_{\mu\nu})}. \quad (22)$$

Using Eqs. (13), (17) and (18), the coefficients $g_{\mu\nu}(z, z_0)$ are solutions of the following relation

$$(\delta_z^2 + k_{z\mu\nu}^2)g_{\mu\nu}(z, z_0) = \delta(z - z_0) \quad \text{for } z \in (0, L) \quad (23)$$

with $k2_{z\mu\nu} = k2 - k_{w\mu\nu}2$. The boundary conditions are given by

$$\partial_z g_{\mu\nu}(z, z_0) = 0 \quad \text{for } z = 0, \quad (24)$$

$$\partial_z g_{\mu\nu}(z, z_0) = 0 \quad \text{for } z = L, \quad (25)$$

and the solution is written

$$g_{\mu\nu}(z, z_0) = -\frac{\cos(k_{z\mu\nu}z)\cos[k_{z\mu\nu}(z_0 - L)]}{k_{z\mu\nu}\sin(k_{z\mu\nu}L)} \quad \text{if } z < z_0, \quad (26)$$

$$g_{\mu\nu}(z, z_0) = -\frac{\cos(k_{z\mu\nu}z_0)\cos[k_{z\mu\nu}(z - L)]}{k_{z\mu\nu}\sin(k_{z\mu\nu}L)} \quad \text{if } z > z_0. \quad (27)$$

4.2. General formulation of acoustic pressure in the volume V

The acoustic pressure in the volume V can now be determined by means of the Green function of the system and the normal acoustic velocity on the surface S. Using Eq. (17) in Eq. (12), the pressure is written as

$$p(\vec{r}) = -j\omega\rho\sum_i\int\int_{S_i}\sum_{\mu,\nu=0}^{\infty}g_{\mu\nu}(z, z_0)\Psi_{\mu\nu}(\vec{w}_0)\Psi_{\mu\nu}(\vec{w})v_{n_i}dS_i, \quad (28)$$

for $i = 1, 2,$ and 3 corresponding, respectively, to the surface S_i and the normal velocities v_{n_i}. Setting

$$p_i(r, \theta, z) = -j\omega\rho\sum_{\mu,\nu=0}^{\infty}\int\int_{S_i}g_{\mu\nu}(z, z_0)\Psi_{\mu\nu}(\vec{w}_0)\Psi_{\mu\nu}(\vec{w})v_{n_i}dS_i \quad (29)$$

the total pressure in the volume V is written as

$$p(r, \theta, z) = \sum_{i=1}^{3}p_i(r, \theta, z) \quad (30)$$

where i indicates the considered surface of the volume. The pressure due to the different surfaces can now be calculated separately to show the influence of each surface area.

4.2.1. Calculation of the pressure field $p_1(r, \theta, z)$

Using Eqs. (20) and (21) in Eq. (29), the pressure field $p_1(r, \theta, z)$ is expressed as

$$p_1(r, \theta, z) = -j\omega\rho\sum_{\mu,\nu=0}^{\infty}g_{\mu\nu}(z, 0)A2_{\mu\nu}\cos(\mu\theta)J_\mu\left(\frac{\gamma_{\mu\nu}}{r_a}r\right)2\pi\delta_{m0}$$
$$\times\int_0^{r_a}v_{n_1}(r_0)J_\mu\left(\frac{\gamma_{\mu\nu}}{r_a}r_0\right)r_0dr_0d\theta_0 \quad (31)$$

where $v_{n_1}(r_0)$, the normal acoustic velocity field for $x = 0$, is independent of θ. Taking into account the cylindrical symmetry of the system, the acoustic pressure field p_1 is also independent of θ (which implies that $\mu = 0$) and is written as

$$p_1(r, z) = -j\omega\rho\sum_{\nu=0}^{\infty}g_{0\nu}(z, 0)A_{0\nu}^2 J_0\left(\frac{\gamma_{0\nu}}{r_a}r\right)2\pi\int_0^{r_a}v_{n_1}(r_0)J_0\left(\frac{\gamma_{0\nu}}{r_a}r_0\right)$$
$$\times r_0dr_0d\theta_0, \quad (32)$$

with

$$g_{0\nu}(z, 0) = -\frac{\cos(k_{z0\nu}(z - L))}{k_{z0\nu}\sin(k_{z0\nu}L)} \quad \text{for } z > 0, \quad (33)$$

and

$$A2_{0\nu} = -\frac{1}{r_a 2\pi J_0(\gamma_{0\nu})}. \quad (34)$$

4.2.2. Calculation of the pressure field $p_2(r, \theta, z)$

The acoustic pressure field $p_2(r, \theta, z)$, considered as independent of θ (due to the cylindrical symmetry), can be expressed as

$$p_2(r, z) = -j\omega\rho\sum_{\nu=0}^{\infty}g_{0\nu}(z, L)A_{0\nu}^2 J_0\left(\frac{\gamma_{0\nu}}{r_a}r\right)2\pi\int_0^{r_a}v_{n_2}(r_0)J_0\left(\frac{\gamma_{0\nu}}{r_a}r_0\right)$$
$$\times r_0dr_0d\theta_0, \quad (35)$$

with

$$g_{0\nu}(z, L) = -\frac{\cos(k_{z0\nu}z)}{k_{z0\nu}\sin(k_{z0\nu}L)} \quad \text{for } z < L, \quad (36)$$

and $A_{0\nu}^2$ defined by Eq. (34).

4.2.3. Calculation of the pressure field $p_3(r, \theta, z)$

The normal acoustic velocity v_{n_3} on the surface S_3, considered as independent of r and θ (due to the cylindrical symmetry), depends only on the z coordinate. The acoustic pressure field $p_3(r, \theta, z)$, considered as independent of θ (due to the cylindrical symmetry), is expressed as a function of the normal acoustic velocity $v_{n_3}(z)$ on the surface S_3 in using Eqs. (20) and (21)

$$p_3(r,z) = -j\omega\rho \sum_{v=0}^{\infty} A_{0v}^2 J_0(\gamma_{0v}) J_0\left(\frac{\gamma_{0v}}{r_a}r\right) 2\pi r_a$$
$$\times \int_0^L v_{n_3}(z_0) g_{0v}(z,z_0) dz_0. \qquad (37)$$

The expression for $g_{0v}(z,z_0)$ depends on the acoustic velocity profile $v_{n_3}(z)$ on the surface S_3.

4.3. Calculation of acoustic pressure in the volume V

Using Eqs. (30), (32), (35) and (37) and, as shown by the experimental results (Section 3.2), considering a incident plane wave on the surface S_1 and $v_{n_2}(r) = 0$ on the surface S_2, the total pressure field in the volume V can be written as

$$p(r,z) = j\omega\rho \frac{\cos[k(z-L)]}{k\sin kL} v_{n_1}$$
$$+ j\frac{2\omega\rho}{r_a}\left(\sum_{v=0}^{\infty}\frac{J_0\left(\frac{\gamma_{0v}}{r_a}r\right)}{J_0(\gamma_{0v})}\frac{1}{k_{z0v}\sin(k_{z0v}L)}\right.$$
$$\times \left\{\cos[k_{z0v}(z-L)]\int_0^z v_{n_3}(z_0)\cos[k_{z0v}z_0]dz_0 + \cos[k_{z0v}z]\right.$$
$$\times \left.\left.\int_z^L v_{n_3}(z_0)\cos[k_{z0v}(z_0-L)]dz_0\right\}\right), \qquad (38)$$

where A_{0v}^2 and $g_{0v}(z,z_0)$ have been substituted by their expressions given by Eqs. (34), (24) and (25).

To express the total pressure field in the volume V, the acoustic velocity profile $v_{n_3}(z)$ on the surface S_3 must be determined. The experimental results (Section 3.2) suggest that this profile can be modeled by a parabolic curve defined as

$$v_{n_3}(z) = -\eta z^2 \text{ for } z \in [0,L] \quad \text{and} \quad \eta > 0. \qquad (39)$$

Finally, the calculation of the integral function in Eq. (38) using Eq. (39) leads to the following result for the total pressure in the volume V

$$p(r,z) = j\omega\rho \frac{\cos[k(z-L)]}{k\sin kL} v_{n_1}$$
$$- j\frac{2\omega\rho}{r_a}\left(\sum_{v=0}^{\infty}\frac{J_0\left(\frac{\gamma_{0v}}{r_a}r\right)}{J_0(\gamma_{0v})}\frac{\eta}{k_{z0v}^2\sin(k_{z0v}L)}\times\left\{z^2\sin(k_{z0v}L)\right.\right.$$
$$+\left.\left.\frac{2}{k_{z0v}}\left[-\frac{1}{k_{z0v}}\sin(k_{z0v}L)+L\cos(k_{z0v}z)\right]\right\}\right), \qquad (40)$$

where $k = k_{z00}$.

Now, the characterization of the acoustic pressure field in the vicinity of the microphone (volume V) can be made with the knowledge of the normal acoustic velocities on the volume boundaries.

5. Results and discussion

The calculation the acoustic pressure in front of the microphone requires the determination of the coefficient of the parabolic curve describing the variation of the normal acoustic velocity on the surface S_3. This coefficient η defined in Eq. (39) is determined by a minimization method. Fig. 8 shows a comparison between the experimental data and the model (defined by Eq. (39)) with $\eta = 135 \text{ m}^{-1} \text{ s}^{-1}$. PIV measurements of the acoustic velocity amplitude normal to S_3 have been obtained for the phase 3 of the acoustic period (see Fig. 3).

Figs. 9 and 10 show the calculation of the pressure amplitude in the volume V for $v = 2$ modes and for $v = 90$ modes, respectively ($v > 0$ corresponds to radial modes defined in Eq. (40)). The influence of the number of modes on the calculation of the acoustic
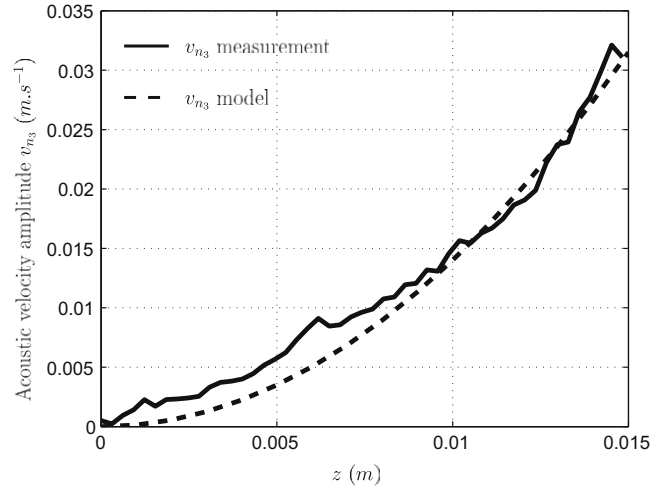

Fig. 8. Normal acoustic velocity amplitude on the surface S_3 as a function of z, experiment (–) and model ($\cdots$) defined by Eq. (39).
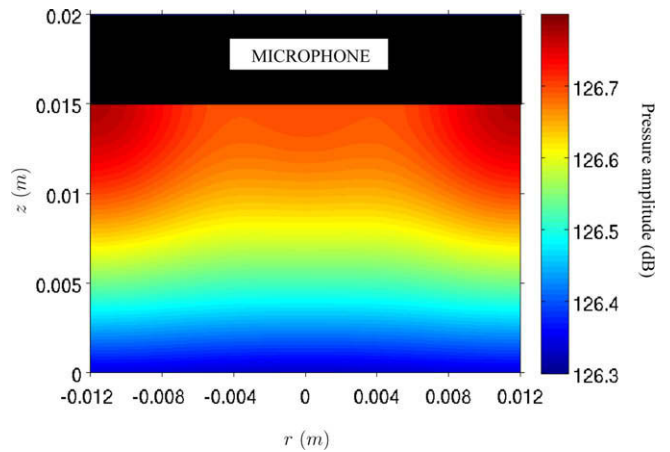

Fig. 9. Calculation of acoustic pressure amplitude in the vicinity of the microphone using Eq. (40) with $v = 2$.
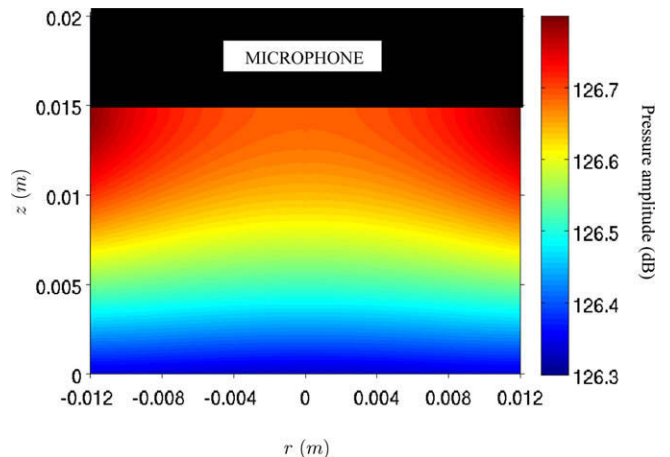

Fig. 10. Calculation of acoustic pressure amplitude in the vicinity of the microphone using Eq. (40) with $v = 90$.

pressure is clearly shown by comparing these two figures. The diffraction effects on the acoustic wave due to the microphone are visible even with 2 modes but this phenomenon is described more

precisely when the modes number increases. According to the experimental results, the presence of the microphone distorts the velocity field streamlines allowing an acoustic leak on the border of the microphone (Fig. 4). This phenomenon leads to an increase of the acoustic pressure amplitude on the edge of the microphone. The acoustic pressure amplitude is not constant along the microphone membrane, varying from 126.65 dB at the microphone center to 126.8 dB at the microphone border. Due to the volume dimension and to the acoustic frequency ($f = 680$ Hz), only the plane mode is propagative and all the higher modes are evanescent. The result of the calculation shows that the microphone edge creates diffraction of the plane wave which leads to the redistribution of the acoustic energy of all the modes and consequently to the excitation of higher modes.

6. Conclusion

A microphone subjected to a plane wave has been studied. Using a propagation model in a fluid domain located close to the microphone membrane and measuring the acoustic velocities on the boundary on the domain provides an estimate of the acoustic pressure on the microphone membrane. This model assumes that the normal acoustic velocity on the microphone membrane is uniformly zero and considers the incident wave as plane.

This preliminary study of the acoustic pressure field in the very close vicinity of a microphone highlights an acoustic pressure gradient along the microphone membrane in order of magnitude of 0.1 dB. This acoustic pressure difference existing between the center and the edge of the membrane can be very problematic when microphone calibration requires an uncertainty less than 0.1 dB. The hypothesis used in this work (incident plane wave, parabolic profile of radial velocity and motionless membrane) tend to minimize this pressure gradient value. A numerical calculation of integrals (Green formulation) would enable to ignore these hypothesis and could lead to a more realistic pressure estimation.

This preliminary study opens new horizons in microphone calibration research, especially in free field conditions. These first results on the acoustic pressure field in the very close vicinity set an important question: what is measured by the microphone since the acoustic pressure is not uniform along the membrane?

In the future, these results should be validated by measuring the acoustic pressure field in the very close vicinity of the microphone using, for instance, a small probe to not perturb the acoustic field. The proposed model can be improved by taking into account the membrane motion which could be estimated using laser probe measurements.

References

[1] Zuckenwar AJ, Herring GC. Calibration of the pressure sensitivity of microphones by e free-field method at frequencies up to 80 kHz. J Acoust Soc Am 2005;119(1):320–9.
[2] International Electrotechnical Commission IEC 61094-2:1992. Measurement microphone – Part 2: primary method for the pressure calibration of laboratory standard microphones by the reciprocity method. International Electrotechnical Commission; 1992.
[3] Barrera Figueroa S, Rasmussen K, Jacobsen F. A time-selective technique for free-field reciprocity calibration of condenser microphones. J Acoust Soc Am 2003;114(3):1467–76.
[4] Barrera Figueroa S, Rasmussen K, Jacobsen F. On the interference between the two microphones in free-field reciprocity calibration. J Acoust Soc Am 2004;116(5):2771–8.
[5] International Electrotechnical Commission IEC 61094-3:1995. Measurement microphone – Part 3: primary method for free field calibration of laboratory standard microphones by the reciprocity method. International Electrotechnical Commission; 1995.
[6] Wagner RP, Nedzelnitsky V. Determination of acoustic center correction values for type LS2aP microphones at normal incidence. J Acoust Soc Am 1998;104(1):192–1203.
[7] Taylor KJ. Absolute calibration of microphone by a laser-Doppler technique. J Acoust Soc Am. 1981;70(4):939–45.
[8] MacGillivray TJ, Campbell DM, Greated CA, Barham R. The development of a microphone calibration technique using laser Doppler anemometry. Acust-Acta Acust 2002;88(1):135–41.
[9] MacGillivray TJ, Campbell DM, Greated CA, Barham R. The development of a microphone calibration technique using photon correlation spectroscopy. Acust-Acta Acust 2003;89(2):369–76.
[10] Koukoulas T, Theobald P, Schlicke T, Barham R. Towards a future primary method for microphone calibration: optical measurement of acoustic velocity in low seeding conditions. Opt Lasers Eng 2008;46:791–6.
[11] Degroot A, MacDonald R, Richoux O, Gazengel B, Campbell M. Suitability of laser Doppler velocimetry for the calibration of pressure microphones. Appl Acoust 2008;69:1308–17.
[12] Gazengel B, Richoux O, Rouquier P. Characterization of a loudspeaker free field radiation by laser doppler velocimetry. Acust-Acta Acust 2007;93(3):447–56.
[13] Schedin S, Wahlin AO, Gren PO. Transient acoustic near field in air generated by impacted plates. J Acoust Soc Am 1996;99(2):700–5.
[14] Moreau S, Boucheron R, Bailliet H, Valire J-C. Mesures LDV et PIV dans les couches limites acoustiques. In: 9^{ieme} Congrès Francophone de Vélocimétrie Laser, Brussels, Belgium; 2004.